
Robust Cross-View Geo-Localization via Content-Viewpoint Disentanglement

Ke Li¹, Di Wang^{1,†}, Xiaowei Wang¹, Zhihong Wu¹, Yiming Zhang²,
Yifeng Wang¹, Quan Wang¹

¹Xidian University ²University of California San Diego

Abstract

Cross-view geo-localization (CVGL) aims to match images of the same geographic location captured from different perspectives, such as drones and satellites. Despite recent advances, CVGL remains highly challenging due to significant appearance changes and spatial distortions caused by viewpoint variations. Existing methods typically assume that cross-view images can be directly aligned within a shared feature space by maximizing feature similarity through contrastive learning. Nonetheless, this assumption overlooks the inherent conflicts induced by viewpoint discrepancies, resulting in extracted features containing inconsistent information that hinders precise localization. In this study, we take a manifold learning perspective and model *the feature space of cross-view images as a composite manifold jointly governed by content and viewpoint information*. Building upon this insight, we propose **CVD**, a new CVGL framework that explicitly disentangles *content* and *viewpoint* factors. To promote effective disentanglement, we introduce two constraints: (i) An intra-view independence constraint, which encourages statistical independence between the two factors by minimizing their mutual information. (ii) An inter-view reconstruction constraint that reconstructs each view by cross-combining *content* and *viewpoint* from paired images, ensuring factor-specific semantics are preserved. As a plug-and-play module, CVD can be seamlessly integrated into existing geo-localization pipelines. Extensive experiments on four benchmarks, *i.e.*, University-1652, SUES-200, CVUSA, and CVACT, demonstrate that CVD consistently improves both localization accuracy and generalization across multiple baselines.

1 Introduction

The widespread deployment of autonomous vehicles, drones, and other intelligent systems has placed growing demands on navigation and localization technologies. To ensure safe and reliable operation, high-precision positioning services have become a fundamental requirement. Cross-view geo-localization (CVGL), an onboard technique independent of external communication infrastructure, offers a promising solution by estimating absolute geospatial coordinates in the absence of conventional localization signals (*e.g.*, GPS) [18, 3, 25, 8]. Given a query image, typically captured from a ground or drone perspective, the goal is to find a matching satellite image from a georeferenced database to infer the query’s location. Most existing approaches formulate CVGL as an image retrieval task [17, 23], training deep neural networks (DNNs) to learn visual similarity across different views. However, the viewpoint disparity between query and satellite imagery introduces severe spatial distortions and appearance variations, making robust matching inherently challenging.

Recent efforts aim to alleviate the viewpoint discrepancy between query and satellite images. A common strategy is to apply predefined geometric transformations to satellite images, such as polar

[†]Corresponding author: wangdi@xidian.edu.cn

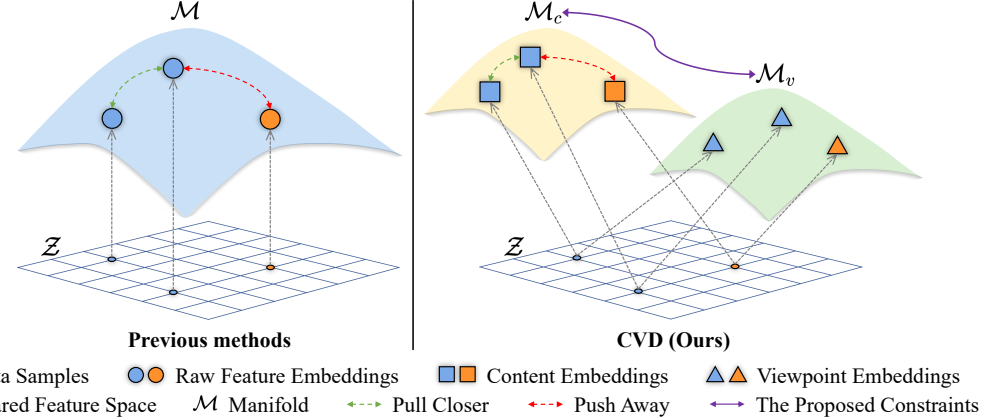


Figure 1: Comparison between previous methods and our CVD. Left: Existing methods can be interpreted as operating on a single manifold \mathcal{M} , where contrastive objectives directly pull positive pairs closer and push negative pairs away. Right: Our method learns disentangled representations by mapping inputs onto two submanifolds corresponding to *content* \mathcal{M}_c and *viewpoint* \mathcal{M}_v . This separation is enforced via two constraints (see Section 3.3 and Section 3.4), promoting effective disentanglement and thereby enhancing cross-view matching performance.

transformation or orthorectification, aligning their spatial layout with that of the query view. However, the effectiveness of these methods relies on prior knowledge of the geometric relationship between views, and may degrade when the query is not spatially centered within the satellite image [31].

Despite recent advances in CVGL, many existing methods [9, 22, 31, 4, 27] still follow a common training paradigm, *i.e.*, directly applying contrastive learning to pull the features of positive pairs closer and push those of negative pairs away. While various architectural or training refinements have been proposed, these methods largely overlook the semantic inconsistencies introduced by drastic viewpoint differences. These inconsistencies disrupt the alignment between positive pairs and ultimately limit the cross-view matching performance.

In this paper, we revisit the CVGL task from a manifold learning perspective by modeling the feature space of cross-view images as a composite manifold jointly governed by *content* and *viewpoint* factors. As illustrated in Figure 1 (left), prior methods can be interpreted as learning representations on a composite manifold \mathcal{M} , where both factors are inherently entangled. Such entanglement introduces viewpoint-induced conflicts into the learned representations, thereby undermining the robustness of contrastive alignment. To address this limitation, we propose **CVD** (Content-Viewpoint Disentanglement), a generic CVGL framework that explicitly factorizes the feature space into two submanifolds: a content submanifold and a viewpoint submanifold (see Figure 1 (right)). The *content* encodes view-agnostic structural information, while the *viewpoint* captures view-specific appearance variations. As shown in Figure 2 (*Training Stage*), CVD adopts an embed-disentangle-reconstruct paradigm. Each image is first embedded into a shared feature space, then projected onto independent content and viewpoint submanifolds, and finally recombined in an image reconstruction task. To facilitate effective disentanglement, we impose two dedicated constraints: an intra-view independence constraint and an inter-view reconstruction constraint. The former encourages statistical independence between *content* and *viewpoint* by minimizing their mutual information, while the latter ensures that each factor retains its intended semantics by reconstructing images using the content of one view and the viewpoint of the other. In addition, we apply a standard contrastive loss (*e.g.*, InfoNCE) to align content representations of matched pairs across views.

To the best of our knowledge, CVD is the first CVGL framework to explicitly disentangle *content* and *viewpoint* information. Unlike existing methods that rely on architectural redesign, CVD serves as a plug-and-play module that can be seamlessly integrated into existing pipelines. It introduces no additional cost during inference while substantially improving matching accuracy and robustness. In summary, our contributions are as follows:

- We revisit the cross-view geo-localization (CVGL) task from a manifold learning perspective and propose CVD, the first framework that explicitly disentangles *content* and *viewpoint* to suppress viewpoint-induced conflicting information.

- We introduce two constraints to facilitate effective disentanglement: an intra-view independence constraint that facilitates the independence between *content* and *viewpoint*, and an inter-view reconstruction constraint that ensures each factor retains its intended semantics.
- CVD can be seamlessly integrated into existing pipelines, incurs no additional inference overhead, and consistently improves cross-view matching performance and generalization across multiple challenging benchmarks.

2 Related Work

CVGL has witnessed significant progress with the availability of large-scale geo-tagged datasets and advances in deep learning. Existing methods predominantly follow a Siamese-based framework and can be broadly categorized into three research directions: data augmentation strategies, architectural innovations, and feature representation learning.

2.1 Data Augmentation Strategies

Data augmentation has become a widely adopted strategy in CVGL tasks [19, 12, 26, 6]. To address cross-view misalignment, Liu *et al.*[9] incorporate camera orientation as auxiliary input, while SAFA[15] applies a polar transformation to align aerial and ground-level panoramas. Several methods further improve robustness by diversifying input image appearances. For instance, Lv *et al.*[10] simulate extreme weather conditions by injecting synthetic variations into University-1652. More recently, training-aware data sampling has emerged as a complementary strategy. Sample4Geo[4] introduces two curriculum-driven strategies: one leveraging geographically adjacent samples for easier early-stage alignment, and another mining hard negatives to refine the decision boundary. Game4Loc [5] proposes a mutual-exclusion sampling mechanism that enforces strict decorrelation between positive and negative pairs, thereby enhancing contrastive supervision in cross-view matching.

2.2 Backbone Innovations

In parallel, a line of work focuses on designing more powerful visual backbones to enhance localization performance [13, 29]. For example, L2LTR [22] exploits self-attention to model long-range dependencies, effectively reducing visual ambiguity in cross-view. RK-Net [7] introduces a lightweight unit-difference attention module that enables joint learning of dense features and salient keypoints, without requiring additional annotations. SAIG [33] proposes an efficient backbone tailored for CVGL by replacing the MLP blocks in standard Transformers with spatially-aware mixing layers and low-dimensional projections, yielding a more compact and structured representation.

2.3 Feature Representation Learning

Many studies focus on learning more effective visual representations to enhance cross-view matching [32, 11, 30, 24]. A common strategy involves refining alignment mechanisms between views. For instance, Shi *et al.*[16] proposed a dynamic similarity matching network to estimate directional alignment, thereby reducing cross-view discrepancies. FSRA[2] leverages transformer-based heatmaps to perform region-level alignment, while LPN [20] incorporates contextual cues via a square-ring partitioning strategy to improve part-based representations. SDPL [1] builds upon LPN by introducing a shifting-fusion mechanism to generate multiple complementary part sets, which are then adaptively aggregated to enhance robustness against spatial shifts and scale variations. Several methods also incorporate inductive priors modeling to enhance feature expressiveness. TransGeo [31] adopts a non-uniform cropping strategy that discards low-information regions while reallocating resolution to semantically salient areas, enhancing accuracy without increasing computational cost. GeoDTR [27] incorporates spatial layout priors through a geometry-aware extraction module, combined with counterfactual training to exploit structural information. MCCG [14] enriches feature diversity by jointly modeling spatial and channel-wise attentions.

Although prior methods perform well across various scenarios, many rely on auxiliary components that increase inference-time overhead. In contrast, we propose a plug-and-play training paradigm that explicitly disentangles *content* and *viewpoint* from raw features, enhancing cross-view correspondence without introducing additional parameters or latency at inference.

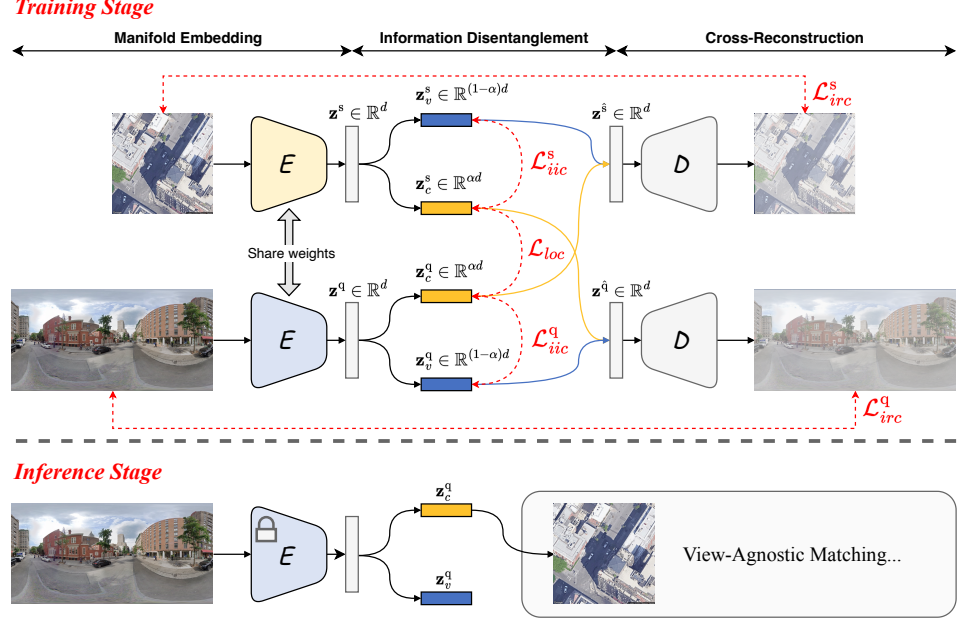


Figure 2: Overview of the proposed CVD.

3 Methodology

3.1 Problem Formulation

Considering a set of image pairs $\{(\mathcal{I}_i^q, \mathcal{I}_i^s)\}_{i=1}^N$, where superscripts q and s denote query (e.g., drone or ground) and satellite images, respectively, and N is the number of pairs. Each pair depicts the same geographic location. In the CVGL task, given a query image \mathcal{I}_q^q with index q , the objective is to retrieve its best-matching satellite image \mathcal{I}_b^s from the georeferenced database, where $b \in \{1, \dots, N\}$.

Most existing methods rely on learning a representation function $f(\cdot)$ that embeds images from different viewpoints into a shared feature space, allowing matching pairs to be identified through feature distance minimization. However, such representations inevitably retain view-specific conflicts, which hinder cross-view semantic alignment and degrade matching performance.

For effective comparison between cross-view images, we aim to modulate raw representations by explicitly disentangling two factors: *content* and *viewpoint*. Concretely, we model the feature space \mathcal{Z} as a representation of *composite manifold* \mathcal{M} structured by two independent submanifolds, \mathcal{M}_c and \mathcal{M}_v , corresponding to *content* and *viewpoint*, respectively. Each feature representation is viewed as a sample from two latent random variables, $C \sim p(C)$ and $V \sim p(V)$, defined over \mathcal{M}_c and \mathcal{M}_v . These are composed via a function $f : \mathcal{M}_c \times \mathcal{M}_v \rightarrow \mathcal{Z}$ that maps both factors to a point in the feature space. Assuming statistical independence between the factors, *i.e.*, $p(C, V) = p(C)p(V)$, the resulting distribution over \mathcal{Z} is given by the push-forward measure $f_{\#}(p(C) \times p(V))$. This assumption is well-aligned with the CVGL task, where identical scenes may be observed under diverse perspectives.

To realize the above formulation, we design manifold encoders that decompose each image \mathcal{I}^u into two distinct representations: a content embedding $f_c(\mathcal{I}^u) \in \mathcal{M}_c$ and a viewpoint embedding $f_v(\mathcal{I}^u) \in \mathcal{M}_v$. Cross-view matching is subsequently performed in the \mathcal{M}_c by retrieving the nearest neighbor of a query image \mathcal{I}_q^q via its content embedding:

$$b = \arg \min_{i \in \{1, \dots, N\}} d(f_c(\mathcal{I}_q^q), f_c(\mathcal{I}_i^s)), \quad (1)$$

where $d(\cdot, \cdot)$ denotes a distance metric. For notation compactness, we will use superscript u ¹ for cases that apply to both query (q) and satellite (s) views.

¹We adopt this convention throughout the paper.

3.2 Proposed Methodology

As illustrated in Figure 2, **CVD** adopts a Siamese architecture consisting of two symmetric branches for the query and satellite views. Each branch comprises three sequential components: manifold embedding, information disentanglement, and cross-reconstruction.

Manifold Embedding. Each input image \mathcal{I}^u ($u \in \{q, s\}$) is first processed by manifold encoders E , yielding a raw d -dimensional feature representations $\mathbf{z}^u = E(\mathcal{I}^u) \in \mathbb{R}^d$. Owing to the nature of DNN encoders, the distribution of \mathbf{z}^u can be viewed as residing on a *composite manifold* jointly governed by *content* and *viewpoint* information. Since our primary focus is on the training paradigm, we adopt the same DNN encoders as those used in the respective baselines to ensure fair and consistent comparisons.

Information Disentanglement. Once we obtain the feature representation \mathbf{z}^u , we project it into two statistically independent components using two parallel 3×3 convolutional layers with a channel ratio of α . One is used to represent the content embedding, denoted as $\mathbf{z}_c^u = f_c(\mathbf{z}^u) \in \mathbb{R}^{\alpha d}$, which provides view-agnostic scene structure. The other is employed for the viewpoint embedding, denoted as $\mathbf{z}_v^u = f_v(\mathbf{z}^u) \in \mathbb{R}^{(1-\alpha)d}$, capturing view-specific attributes. To promote effective disentanglement, we introduce an *intra-view independence constraint* (Section 3.3) that minimizes the mutual information $\text{MI}(Z_c^u; Z_v^u)$, where Z^u denotes the random variables of \mathbf{z}^u , thereby encouraging statistical independence between *content* and *viewpoint* factors.

Cross-Reconstruction. While the independence constraint enhances factor separation, it may inadvertently lead to degenerate solutions or information loss. To mitigate this, we introduce an *inter-view reconstruction constraint* that encourages each factor to retain its intended information through cross-view image reconstruction. Specifically, we train two decoders, D^q and D^s , to perform bidirectional reconstruction between paired views by swapping content and viewpoint embeddings, *i.e.*, reconstructing each image using its own viewpoint and the content of the other. By enforcing accurate reconstruction from these hybrid embeddings, the model is incentivized to encode factor-specific information in each representation. This cross-view supervision not only prevents information collapse but also reinforces disentanglement. In the following, we describe the two specific constraints in CVD.

3.3 Intra-view Independence Constraint

To effectively disentangle *content* and *viewpoint* factors, we introduce an intra-view independence constraint that aims to minimize the statistical dependence between the two embeddings. Motivated by the principle that mutual information provides a fundamental measure of statistical dependence, we seek to encourage independent factorization by minimizing it between *content* and *viewpoint*.

Formally, the mutual information between Z_c^u and Z_v^u is defined as the Kullback-Leibler (KL) divergence between their joint distribution and the product of marginals:

$$\text{MI}(Z_c^u; Z_v^u) = \mathcal{D}_{\text{KL}}(p(\mathbf{z}_c^u, \mathbf{z}_v^u) \parallel p(\mathbf{z}_c^u)p(\mathbf{z}_v^u)). \quad (2)$$

However, direct computation or optimization of mutual information is notoriously intractable in high-dimensional feature spaces due to the need for accurate estimation of joint and marginal densities. To circumvent this issue, we adopt the *Sliced Wasserstein Distance* (SWD) as a geometry-aware and sample-efficient proxy to promote independence. Specifically, we minimize the SWD between the empirical joint distribution $p(\mathbf{z}_c^u, \mathbf{z}_v^u)$ and the product of its marginals $p(\mathbf{z}_c^u)p(\mathbf{z}_v^u)$, which can be represented as:

$$\mathcal{L}_{\text{iic}}^u = \mathcal{SW}_2(p(\mathbf{z}_c^u, \mathbf{z}_v^u), p(\mathbf{z}_c^u) \otimes p(\mathbf{z}_v^u)), \quad (3)$$

where $\mathcal{SW}_2(\cdot, \cdot)$ denotes the Sliced Wasserstein-2 distance. We apply this constraint independently to both views, yielding $\mathcal{L}_{\text{iic}}^q$ and $\mathcal{L}_{\text{iic}}^s$. This constraint drives the separation of view-agnostic scene structure from view-specific attributes in a computationally tractable manner.

3.4 Inter-view Reconstruction Constraint

While the independence constraint promotes factor separation, it does not guarantee that each embedding retains the essential factor-specific information. In particular, relying solely on independence may lead to trivial solutions where either the content or viewpoint embedding becomes uninformative.

To address this, we introduce an *inter-view reconstruction constraint* that enforces information retention through cross-view image reconstruction. Specifically, we deploy decoders D that reconstruct each image from a hybrid embedding composed of *content* from one view with the *viewpoint* from the other, which is denoted as:

$$\hat{\mathcal{I}}^q = D^q(\mathbf{z}_c^s, \mathbf{z}_v^q), \quad \hat{\mathcal{I}}^s = D^s(\mathbf{z}_c^q, \mathbf{z}_v^s). \quad (4)$$

This constraint ensures that both \mathbf{z}_c^u and \mathbf{z}_v^u preserve distinct and sufficient information, thereby preventing representational collapse. Notably, the reconstruction is conditioned on the *viewpoint*, which governs spatial and geometric layout, while the *content* determines underlying scene structure. The reconstruction loss is defined as:

$$\mathcal{L}_{irc}^u = \|\mathcal{I}^u - \hat{\mathcal{I}}^u\|_2^2. \quad (5)$$

where $\|\cdot\|_2^2$ denotes the mean squared error (MSE) between the original and reconstructed images. This loss is also applied to both views, resulting in \mathcal{L}_{irc}^q and \mathcal{L}_{irc}^s , which ensure that the disentangled features preserve the necessary information to reconstruct their cross-view counterparts.

3.5 Training Objective

Following prior works [4, 11], we employ the standard InfoNCE loss for view-agnostic content consistency across views, denoted as \mathcal{L}_{loc} , which encourages *content* of matched query-satellite pairs to be close while pushing away mismatched pairs, and is defined as:

$$\mathcal{L}_{loc} = -\log \frac{\exp(\mathbf{z}_c^q \cdot \mathbf{z}_c^s / \tau)}{\sum_{i=1}^N \exp(\mathbf{z}_c^q \cdot \mathbf{z}_c^i / \tau)}, \quad (6)$$

where τ is a temperature parameter that controls the sharpness of the similarity distribution. The overall training objective for CVD combines three losses: (1) an intra-view independence loss \mathcal{L}_{iic}^u promotes *content* and *viewpoint* independence, (2) an inter-view reconstruction loss \mathcal{L}_{irc}^u to ensure intended information preservation, and (3) a cross-view localization loss \mathcal{L}_{loc} for discriminative alignment, which can be expressed as:

$$\mathcal{L}_{total} = \lambda_1 \left(\frac{1}{2} \mathcal{L}_{iic}^q + \frac{1}{2} \mathcal{L}_{iic}^s \right) + \lambda_2 \left(\frac{1}{2} \mathcal{L}_{irc}^q + \frac{1}{2} \mathcal{L}_{irc}^s \right) + \lambda_3 \mathcal{L}_{loc}, \quad (7)$$

where λ_1 , λ_2 , and λ_3 are hyperparameters that balance the three losses during training.

4 Experiments

4.1 Settings

Datasets. We evaluate our method on four representative CVGL benchmarks: University-1652 [28], SUES-200 [30], CVUSA [21], and CVACT_val [9], which collectively encompass various perspective combinations, including ground-view, drone-view, and satellite-view imagery. **University-1652** comprises images from 1,652 university campuses captured in ground, drone, and satellite views. In our experiments, we adopt the drone-satellite setting, using 701 campuses for training, 701 for testing, along with 250 distractor samples. **SUES-200** consists of real-world drone and satellite imagery from 200 scenes across four altitudes (150-300m), with 120 scenes for training and 80 for testing. **CVUSA** and **CVACT_val** provide large-scale ground-satellite image pairs, with 35,532 aligned in the training set for each. The former contains 8,884 test queries, while the latter offers a validation set of the same size.

Evaluation metrics. We adopt five standard retrieval metrics, including Average Precision (AP), Recall@K (K=1,5,10), and Recall@1%, to evaluate cross-view matching performance. Detailed definitions of metrics can be found in the Appendix.

Implementation details. The hyperparameters of the total training loss \mathcal{L}_{total} are fixed across all models and datasets, with $\lambda_1 = 10$, $\lambda_2 = 0.2$, and $\lambda_3 = 1$. The temperature parameter τ is set to 0.05. To ensure fair comparisons, we strictly follow the original training configurations of each baseline, including optimizer type, learning rate schedule, batch size, *etc.*, without any additional tuning. All experiments are conducted in PyTorch on an NVIDIA RTX 4090 GPU with 24 GB memory.

Table 1: Comparison between CVD and baseline methods on University-1652. ‘†’ represents that CVD is applied during training.

Method	Image Size	Backbone	Drone → Satellite					Satellite → Drone				
			AP	R@1	R@5	R@10	R@1%	AP	R@1	R@5	R@10	R@1%
LPN	256×256	ResNet50	77.26	73.87	88.84	92.58	93.01	73.55	85.28	89.27	91.15	98.29
LPN†	256×256	ResNet50	78.99	75.78	89.96	93.45	93.81	74.89	85.88	90.73	92.58	99.00
SDPL	512×512	ResNet50	86.45	84.13	94.36	96.45	96.72	82.17	89.44	92.58	93.58	99.29
SDPL†	512×512	ResNet50	87.24	84.98	95.21	96.91	97.19	82.98	89.83	93.15	94.58	99.43
MCCG	256×256	ConvNeXt-T	90.63	88.92	96.44	97.63	97.77	88.73	93.15	95.72	96.72	99.57
MCCG†	256×256	ConvNeXt-T	92.19	90.67	97.65	98.55	98.67	89.63	93.65	96.71	97.84	99.68
Sample4Geo	384×384	ConvNeXt-B	93.56	92.36	97.64	98.26	98.36	91.64	94.72	97.00	97.43	99.43
Sample4Geo†	384×384	ConvNeXt-B	94.78	93.73	98.56	98.90	98.95	92.48	95.26	97.76	98.47	99.55
Game4Loc	384×384	ViT-B	92.56	91.32	96.56	97.33	97.41	90.83	94.43	95.72	96.57	98.71
Game4Loc†	384×384	ViT-B	93.95	92.94	97.59	98.28	98.32	91.92	94.86	96.71	97.14	99.57

4.2 Results on University-1652

To evaluate the effectiveness of CVD, we integrate it into five representative baselines spanning diverse architectures, including ResNet, ConvNeXt, and Vision Transformer (ViT), and conduct experiments on University-1652. As summarized in Table 1, CVD consistently improves performance across all backbones and evaluation metrics. For instance, incorporating CVD into MCCG yields a +1.75% improvement in R@1 (Drone→Satellite), while Game4Loc shows notable gains of +1.39% in AP and +1.62% in R@1. Note that CVD is used only during training and introduces no additional inference overhead. These results support our hypothesis that explicitly disentangling *content* and *viewpoint* leads to more robust and discriminative representations for cross-view geo-localization.

Table 2: Comparison between CVD and baseline methods on SUES-200. ‘†’ represents that CVD is applied during training.

Method	Drone → Satellite								Satellite → Drone							
	150m		200m		250m		300m		150m		200m		250m		300m	
	AP	R@1	AP	R@1	AP	R@1	AP	R@1	AP	R@1	AP	R@1	AP	R@1	AP	R@1
LPN	63.50	58.20	74.16	69.60	79.70	75.60	82.93	78.50	63.68	77.50	78.36	87.50	84.26	90.00	87.99	92.50
LPN †	64.24	59.77	74.39	70.38	81.14	77.50	84.26	79.38	64.88	78.40	80.13	88.74	85.50	93.75	89.72	93.41
FSRA	69.31	66.86	84.79	82.43	90.74	88.50	92.55	90.12	74.99	78.53	88.04	89.89	91.76	92.51	92.30	95.10
FSRA †	70.51	67.97	85.22	83.07	92.11	89.90	93.76	91.70	76.45	79.40	89.04	91.07	92.98	94.26	92.90	95.99
SDPL	76.64	72.07	84.98	81.92	89.53	87.05	92.34	90.35	70.28	80.00	80.57	86.25	85.64	88.75	87.43	90.00
SDPL †	77.11	75.30	85.19	83.00	91.25	88.99	92.97	90.86	71.43	80.80	81.84	87.10	85.81	91.25	88.52	91.25
MCCG	81.21	79.96	86.24	85.01	92.15	90.47	94.97	94.20	89.76	92.06	92.40	93.88	96.15	96.34	96.52	98.78
MCCG †	82.10	80.56	87.16	86.40	92.98	91.08	95.37	94.84	90.92	92.96	93.15	94.44	96.43	97.06	96.74	98.99
MBF	84.52	82.19	87.41	85.27	90.85	89.62	92.60	91.33	83.96	86.36	89.93	91.39	90.90	92.95	91.60	96.25
MBF †	85.24	83.19	88.20	85.52	91.90	90.46	93.48	92.09	85.11	86.97	91.00	92.51	92.23	93.80	91.80	96.98
Game4Loc	95.59	94.62	97.27	96.55	98.16	97.55	98.24	97.67	93.06	93.75	94.50	96.25	94.92	96.25	95.36	95.00
Game4Loc †	96.70	95.80	97.78	97.10	98.14	97.60	98.98	98.65	93.37	96.25	95.03	97.50	95.95	96.25	96.28	97.50

4.3 Results on SUES-200

We evaluate CVD on SUES-200 to examine its robustness under varying levels of viewpoint disparity induced by different drone altitudes. As reported in Table 2, CVD improves the performance of all baselines across both matching directions and all altitude levels. Notably, the relative gains are more pronounced at lower altitudes (*e.g.*, 150m), where off-nadir distortions are most severe. At this height, FSRA and LPN improve by +1.46% and +1.20% in AP (Satellite→Drone), while SDPL sees a +2.69% gain in R@1 (Drone→Satellite). As altitude increases and the viewpoint gap narrows, CVD continues to yield consistent improvements. For instance, MBF and MCCG achieve +0.88% and +0.40% gains in AP at 300m. These results demonstrate that CVD enhances localization robustness under diverse spatial conditions, particularly in low-altitude settings where viewpoint-induced distortions are most challenging.

4.4 Results on CVUSA and CVACT

We further evaluate CVD on CVUSA and CVACT, which involve ground-to-satellite matching under extreme viewpoint differences and substantial scene layout variation. As shown in Table 3, all baselines exhibit measurable improvements when trained with CVD, even though they already perform strongly. These improvements are particularly meaningful given the challenges posed by ground-view imagery, such as occlusion, illumination changes, and perspective distortion.

Table 3: Comparison between CVD and baseline methods on CVUSA and CVACT. ‘†’ represents that CVD is applied during training.

Method	CVUSA				CVACT_val			
	R@1	R@5	R@10	R@1%	R@1	R@5	R@10	R@1%
LPN	85.43	95.20	96.91	99.40	78.86	89.97	92.07	95.34
LPN †	87.15	96.43	97.26	99.49	80.08	91.10	93.16	96.69
TransGeo	93.72	98.01	98.56	99.78	83.99	93.49	95.17	97.80
TransGeo †	94.35	98.83	99.07	99.80	84.96	94.61	95.90	98.44
GeoDTR	93.05	98.01	98.94	99.80	85.11	94.00	95.47	98.03
GeoDTR †	93.92	98.70	99.26	99.83	85.72	95.19	96.63	98.74
Sample4Geo	98.43	99.15	99.42	99.81	90.29	95.98	97.04	98.53
Sample4Geo †	98.67	99.40	99.78	99.89	90.94	96.80	97.51	98.81

By explicitly separating view-specific conflicting information, CVD enhances the consistency of content representations across modalities. For example, Sample4Geo improves by +0.24% and +0.65% in R@1 on CVUSA and CVACT, respectively, while GeoDTR achieves +0.77% and +0.61% gains in R@10.

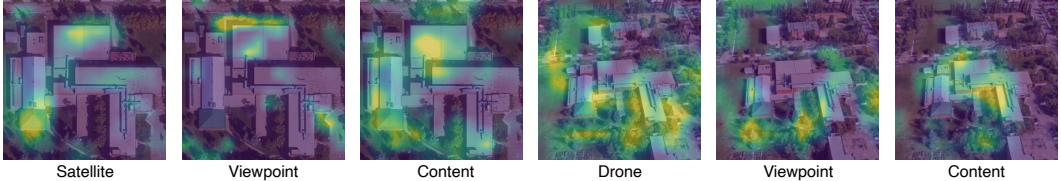


Figure 3: Visualization of disentangled *content* and *viewpoint* attention maps produced by CVD.

4.5 Visualization of Disentangled Embeddings

Figure 3 visualizes attention maps derived from the disentangled embeddings produced by CVD. Viewpoint embeddings predominantly focus on peripheral, view-specific elements such as vegetation, shadows, and roads, which are often inconsistent across modalities. In contrast, content embeddings attend to semantically stable regions like building structures, providing reliable and discriminative cues for cross-view matching. This separation facilitates CVD to learn robust, viewpoint-agnostic content representations, thereby improving retrieval under significant viewpoint disparity. More visualizations are given in the Appendix.

Table 4: Ablation of the components of CVD.

Exp.	Methods (ResNet50)	D → S		S → D	
		AP	R@1	AP	R@1
1	Baseline LPN	77.26	73.87	73.55	85.28
2	w/o two constraints	74.62	71.83	69.85	83.49
3	Exp.1 + iic loss	77.95	73.95	73.97	85.24
4	Exp.1 + irc loss	78.28	74.62	74.63	85.45
5	CVD (LPN)	78.99	75.78	74.89	85.88
6	Baseline Game4Loc	72.90	68.49	66.53	83.16
7	w/o two constraints	69.71	65.85	64.51	81.19
8	Exp.6 + iic loss	73.29	69.19	66.70	83.20
9	Exp.7 + irc loss	73.60	69.78	67.03	83.61
10	CVD (Game4Loc)	74.31	70.46	67.60	83.67

Table 5: Ablation of content-viewpoint ratio.

Split Ratio	D → S		S → D	
	AP	R@1	AP	R@1
$\alpha = 1/3$	78.13	74.90	74.08	84.31
$\alpha = 1/2$	78.99	75.78	74.89	85.88
$\alpha = 3/4$	78.15	74.76	73.28	86.59
No squeeze	78.06	74.85	74.48	84.85

Table 6: Influence of different τ in InfoNCE.

Method	D → S		S → D	
	AP	R@1	AP	R@1
$\tau = 0.07$	78.89	75.74	74.28	85.03
$\tau = 0.05$	78.99	75.78	74.89	85.88
$\tau = 0.03$	78.98	75.76	74.61	85.43
Bi-InfoNCE	78.72	75.14	74.36	85.21

4.6 Ablation Study

Effectiveness of CVD. We conduct ablation studies on University-1652 to evaluate the contribution of each component in CVD, as summarized in Table 4. To ensure fair comparison, we adopt two representative pipelines, LPN and Game4Loc, which both use a shared ResNet50 backbone. Removing both constraints (Exp.2 and 7) leads to a notable performance drop, while individually adding the intra-view independence (Exp.3 and 8) or inter-view reconstruction constraint (Exp.4 and 9) yields consistent gains. The best results are obtained when both constraints are jointly applied (Exp.5 and 10), confirming that explicitly factorizing *content* and *viewpoint* is essential for robust cross-view alignment.

Content-Viewpoint Ratio. We investigate the impact of different split ratios between content embedding and viewpoint embedding, as reported in Table 5. Assigning an imbalanced proportion of dimensions, favoring either content ($\alpha = 3/4$) or viewpoint ($\alpha = 1/3$), results in performance drops of 0.84% and 0.81% in AP (Drone → Satellite), respectively. The best performance occurs when $\alpha = 1/2$, indicating that balanced factorization most effectively preserves factor-specific information. Interestingly, the ‘No squeeze’ setting, where both branches retain full dimensionality,

also underperforms the balanced configuration by 0.93% in AP, suggesting that moderate compression encourages more effective disentanglement.

Temperature Parameter Analysis. As shown in Table 6, model performance remains stable across a range of temperature values τ . This insensitivity indicates that the performance gains primarily result from effective representation disentanglement rather than contrastive loss tuning.

Table 7: Generalization ablation when trained on University-1652 and tested on SUES-200. ‘†’ represents that CVD is applied during training.

Method	Drone → Satellite										Satellite → Drone									
	150m					200m					250m					300m				
	AP	R@1	AP	R@1	AP	AP	R@1	AP	R@1	AP	AP	R@1	AP	R@1	AP	R@1	AP	R@1	AP	R@1
LPN	42.83	36.70	52.99	46.72	59.42	53.62	62.15	56.55	25.30	30.00	34.36	38.75	38.53	42.50	43.92	53.75				
LPN †	44.93	38.58	56.68	50.50	62.16	55.73	64.89	58.60	29.21	32.50	39.18	42.50	45.98	52.50	52.52	60.00				
Game4Loc	82.39	78.85	88.57	86.10	90.31	88.17	90.94	88.75	75.29	80.00	81.31	88.75	84.31	88.75	86.40	92.50				
Game4Loc †	86.12	82.87	91.77	89.70	93.59	91.92	94.44	92.92	75.37	87.50	84.25	90.00	87.97	95.00	90.21	95.00				

4.7 Generalisation Capabilities

To evaluate the generalization ability of CVD to unseen scenes, we train models on University-1652 and directly evaluate them on SUES-200 without any fine-tuning. As shown in Table 7, CVD significantly improves performance across all metrics for both LPN (ResNet-50) and Game4Loc (ViT-B). For example, it boosts R@1 by up to +6.25% for LPN and +7.5% for Game4Loc, even without access to the target domain during training. Remarkably, these cross-dataset improvements exceed those typically obtained via in-domain training on SUES-200, which yields only improvements of 1-3%. These results highlight that disentangling *content* and *viewpoint* leads to more transferable representations that generalize effectively across regions and views.

4.8 Effectiveness of Content-Viewpoint Disentanglement

To further evaluate the effectiveness of disentangling *content* and *viewpoint*, we conduct a cross-view recombination experiment using the learned embeddings. As illustrated in Figure 4, each row shows two reconstructed heatmaps, which share the same *content* but differ in the *viewpoint*. In the top row, the same satellite content embedding is combined with either a matched (left) or unrelated (right) drone viewpoint; in the bottom row, drone content is paired with matched and unrelated satellite viewpoints, respectively. Despite the change in viewpoint, the resulting attention maps exhibit similar attention patterns, highlighting semantically consistent regions. These results provide qualitative evidence that CVD effectively disentangles the two factors: content embeddings encode view-agnostic structural information, while viewpoint embeddings modulate geometric and contextual variations. More visualizations are provided in the Appendix.

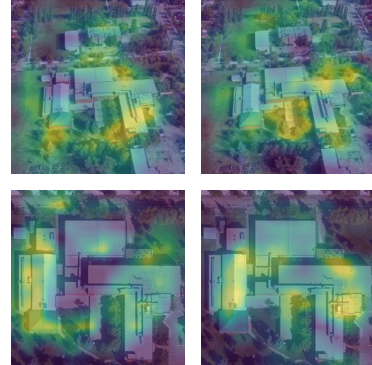


Figure 4: Cross-view reconstructions with matched (left column) and unrelated (right column) viewpoints.

5 Conclusion and Limitations

In this paper, we revisit cross-view geo-localization (CVGL) from a manifold learning perspective and propose **CVD**, a unified framework that explicitly disentangles *content* and *viewpoint* within the visual representation. CVD adopts an embed-disentangle-reconstruct paradigm, guided by intra-view independence and inter-view reconstruction constraints, to promote *content*- and *viewpoint*-specific encoding. Extensive experiments demonstrate that CVD consistently enhances both localization accuracy and generalization across diverse CVGL pipelines. These findings underscore the value of explicitly separating *content* and *viewpoint* in CVGL, and offer insights toward developing more robust and generalizable CVGL systems. A discussion of limitations and potential future directions is provided in the Appendix.

References

- [1] Quan Chen, Tingyu Wang, Zihao Yang, Haoran Li, Rongfeng Lu, Yaoqi Sun, Bolun Zheng, and Chenggang Yan. Sdpl: Shifting-dense partition learning for uav-view geo-localization. *IEEE Transactions on Circuits and Systems for Video Technology*, 2024.
- [2] Ming Dai, Jianhong Hu, Jiedong Zhuang, and Enhui Zheng. A transformer-based feature segmentation and region alignment method for uav-view geo-localization. *IEEE Transactions on Circuits and Systems for Video Technology*, 32(7):4376–4389, 2021.
- [3] Ming Dai, Enhui Zheng, Zhenhua Feng, Lei Qi, Jiedong Zhuang, and Wankou Yang. Vision-based uav self-positioning in low-altitude urban environments. *IEEE Transactions on Image Processing*, 33:493–508, 2023.
- [4] Fabian Deuser, Konrad Habel, and Norbert Oswald. Sample4geo: Hard negative sampling for cross-view geo-localisation. In *Proceedings of the IEEE/CVF International Conference on Computer Vision*, pages 16847–16856, 2023.
- [5] Yuxiang Ji, Boyong He, Zhuoyue Tan, and Liaoni Wu. Game4loc: A uav geo-localization benchmark from game data. In *Proceedings of the AAAI Conference on Artificial Intelligence*, volume 39, pages 3913–3921, 2025.
- [6] Guopeng Li, Ming Qian, and Gui-Song Xia. Unleashing unlabeled data: A paradigm for cross-view geo-localization. In *Proceedings of the IEEE/CVF Conference on Computer Vision and Pattern Recognition*, pages 16719–16729, 2024.
- [7] Jinliang Lin, Zhedong Zheng, Zhun Zhong, Zhiming Luo, Shaozi Li, Yi Yang, and Nicu Sebe. Joint representation learning and keypoint detection for cross-view geo-localization. *IEEE Transactions on Image Processing*, 31:3780–3792, 2022.
- [8] Tsung-Yi Lin, Yin Cui, Serge Belongie, and James Hays. Learning deep representations for ground-to-aerial geolocation. In *Proceedings of the IEEE conference on computer vision and pattern recognition*, pages 5007–5015, 2015.
- [9] Liu Liu and Hongdong Li. Lending orientation to neural networks for cross-view geo-localization. In *Proceedings of the IEEE/CVF conference on computer vision and pattern recognition*, pages 5624–5633, 2019.
- [10] Hongxiang Lv, Hai Zhu, Mengmeng Xu, Enlai Dong, Fei Wu, and Yueyue Fan. Weln: Siamese network-based framework for geo-localization in extreme weather. In *Proceedings of the 2nd Workshop on UAVs in Multimedia: Capturing the World from a New Perspective*, pages 4–8, 2024.
- [11] Li Mi, Chang Xu, Javiera Castillo-Navarro, Syrielle Montariol, Wen Yang, Antoine Bosselut, and Devis Tuia. Congeo: Robust cross-view geo-localization across ground view variations. In *European Conference on Computer Vision*, pages 214–230. Springer, 2024.
- [12] Royston Rodrigues and Masahiro Tani. Are these from the same place? seeing the unseen in cross-view image geo-localization. In *Proceedings of the IEEE/CVF Winter Conference on Applications of Computer Vision*, pages 3753–3761, 2021.
- [13] Royston Rodrigues and Masahiro Tani. Global assists local: Effective aerial representations for field of view constrained image geo-localization. In *Proceedings of the IEEE/CVF Winter Conference on Applications of Computer Vision*, pages 3871–3879, 2022.
- [14] Tianrui Shen, Yingmei Wei, Lai Kang, Shanshan Wan, and Yee-Hong Yang. Mccg: A convnext-based multiple-classifier method for cross-view geo-localization. *IEEE Transactions on Circuits and Systems for Video Technology*, 34(3):1456–1468, 2023.
- [15] Yujiao Shi, Liu Liu, Xin Yu, and Hongdong Li. Spatial-aware feature aggregation for cross-view image based geo-localization. In *Proceedings of the 33rd Annual Conference on Neural Information Processing Systems, NeurIPS 2019*, pages 10090–10100.

[16] Yujiao Shi, Xin Yu, Dylan Campbell, and Hongdong Li. Where am i looking at? joint location and orientation estimation by cross-view matching. In *Proceedings of the IEEE/CVF Conference on Computer Vision and Pattern Recognition*, pages 4064–4072, 2020.

[17] Yuxi Sun, Shanshan Feng, Yunming Ye, Xutao Li, Jian Kang, Zhichao Huang, and Chuyao Luo. Multisensor fusion and explicit semantic preserving-based deep hashing for cross-modal remote sensing image retrieval. *IEEE Transactions on Geoscience and Remote Sensing*, 60:1–14, 2021.

[18] Yuxi Sun, Yunming Ye, Jian Kang, Ruben Fernandez-Beltran, Shanshan Feng, Xutao Li, Chuyao Luo, Puzhao Zhang, and Antonio Plaza. Cross-view object geo-localization in a local region with satellite imagery. *IEEE Transactions on Geoscience and Remote Sensing*, 61:1–16, 2023.

[19] Nam N Vo and James Hays. Localizing and orienting street views using overhead imagery. In *European conference on computer vision*, pages 494–509. Springer, 2016.

[20] Tingyu Wang, Zhedong Zheng, Chenggang Yan, Jiyong Zhang, Yaoqi Sun, Bolun Zheng, and Yi Yang. Each part matters: Local patterns facilitate cross-view geo-localization. *IEEE Transactions on Circuits and Systems for Video Technology*, 32(2):867–879, 2021.

[21] Scott Workman, Richard Souvenir, and Nathan Jacobs. Wide-area image geolocalization with aerial reference imagery. In *Proceedings of the IEEE International Conference on Computer Vision*, pages 3961–3969, 2015.

[22] Hongji Yang, Xiufan Lu, and Yingying Zhu. Cross-view geo-localization with layer-to-layer transformer. *Advances in Neural Information Processing Systems*, 34:29009–29020, 2021.

[23] Junyan Ye, Zhutao Lv, Weijia Li, Jinhua Yu, Haote Yang, Huaping Zhong, and Conghui He. Cross-view image geo-localization with panorama-bev co-retrieval network. In *European Conference on Computer Vision*, pages 74–90. Springer, 2024.

[24] Menghua Zhai, Zachary Bessinger, Scott Workman, and Nathan Jacobs. Predicting ground-level scene layout from aerial imagery. In *Proceedings of the IEEE Conference on Computer Vision and Pattern Recognition*, pages 867–875, 2017.

[25] Qingwang Zhang and Yingying Zhu. Aligning geometric spatial layout in cross-view geo-localization via feature recombination. In *Proceedings of the AAAI Conference on Artificial Intelligence*, volume 38, pages 7251–7259, 2024.

[26] Qingwang Zhang and Yingying Zhu. Benchmarking the robustness of cross-view geo-localization models. In *European Conference on Computer Vision*, pages 36–53. Springer, 2024.

[27] Xiaohan Zhang, Xingyu Li, Waqas Sultani, Yi Zhou, and Safwan Wshah. Cross-view geo-localization via learning disentangled geometric layout correspondence. In *Proceedings of the AAAI conference on artificial intelligence*, volume 37, pages 3480–3488, 2023.

[28] Zhedong Zheng, Yunchao Wei, and Yi Yang. University-1652: A multi-view multi-source benchmark for drone-based geo-localization. In *Proceedings of the 28th ACM international conference on Multimedia*, pages 1395–1403, 2020.

[29] Runzhe Zhu, Mingze Yang, Kaiyu Zhang, Fei Wu, Ling Yin, and Yujin Zhang. Modern backbone for efficient geo-localization. In *Proceedings of the 2023 Workshop on UAVs in Multimedia: Capturing the World from a New Perspective*, pages 31–37, 2023.

[30] Runzhe Zhu, Ling Yin, Mingze Yang, Fei Wu, Yuncheng Yang, and Wenbo Hu. Sues-200: A multi-height multi-scene cross-view image benchmark across drone and satellite. *IEEE Transactions on Circuits and Systems for Video Technology*, 33(9):4825–4839, 2023.

[31] Sijie Zhu, Mubarak Shah, and Chen Chen. Transgeo: Transformer is all you need for cross-view image geo-localization. In *Proceedings of the IEEE/CVF Conference on Computer Vision and Pattern Recognition*, pages 1162–1171, 2022.

[32] Sijie Zhu, Taojiannan Yang, and Chen Chen. Vigor: Cross-view image geo-localization beyond one-to-one retrieval. In *Proceedings of the IEEE/CVF Conference on Computer Vision and Pattern Recognition*, pages 3640–3649, 2021.

[33] Yingying Zhu, Hongji Yang, Yuxin Lu, and Qiang Huang. Simple, effective and general: A new backbone for cross-view image geo-localization. *arXiv preprint arXiv:2302.01572*, 2023.